Earthquakes and Structures, *Vol. 17, No. 6 (2019) 611-621*
DOI: https://doi.org/10.12989/eas.2019.17.6.611

Seismic performance of precast joint in assembled monolithic station: effect of assembled seam shape and position

Hongtao Liu[1,2a] and Xiuli Du[*1]

[1]*Key Laboratory of Urban Security and Disaster Engineering of the Ministry of Education, Beijing University of Technology, Beijing 100124, China*
[2]*Faculty of Construction and Environment Department of Building and Real Estate, Hong Kong Polytechnic University, Hong Kong, 999077, China*

(*Received April 4, 2019, Revised October 28, 2019, Accepted November 9, 2019*)

Abstract. Precast concrete structure has many advantages, but the assembled seam will affect potentially the overall seismic performance of structure. Based on the sidewall joint located in the bottom of assembled monolithic subway station, the main objectives of this study are, on one hand to present an experimental campaign on the seismic behavior of precast sidewall joint (PWJ) and cast-in-place sidewall joint (CWJ) subjected to low-cycle repeated loading, and on the other hand to explore the effect of shape and position of assembled seam on load carrying capacity and crack width of precast sidewall joint. Two full-scale specimens were designed and tested. The important index of failure pattern, loading carrying capacity, deformation performance and crack width were evaluated and compared. Based on the test results, a series of different height and variably-shape of assembled seam of precast sidewall joint were considered. The test and numerical investigations indicate that, (1) the carrying capacity and deformation capacity of precast sidewall and cast-in-place sidewall were very similar, but the crack failure pattern, bending deformation and shearing deformation in the plastic hinge zone were different obviously; (2) the influence of the assembled seam should be considered when precast underground structures located in the aquifer water-bearing stratum; (3) the optimal assembled seam shape and position can be suggested for the design of precast underground concrete structures according to the analysis results.

Keywords: precast sidewall joint; low-cycle repeated loading experiment; numerical analysis; assembled seam shape; assembled seam position; seismic performance

1. Introduction

Precast concrete is accepted as unique advantage of saved construction time and cost, insured better quality control and environmental protection etc. (Choi *et al*. 2013, Akköse *et al*. 2018, Nzabonimpa and Hong 2019, Rave-Arango *et al*. 2018). Regular practical implementation of precast systems was utilized in various countries around the world. Comparing with cast-in-place concrete structures, the main challenge in the design of precast concrete structure was in finding reasonable construction method for connecting the precast element together (Park 1995, Beilic *et al*. 2017). To some extent, the overall performance of precast concrete structures were affected by the assembled seam. An improved understanding of the deformation and failure mechanisms of underground structure (Ma *et al*. 2018) caused by seismic cyclic load is essential to recommend that the precast structures was more suitable for underground structure compared with that of cast-in-place structures. However, the unavoidably assembled seam in the precast structure could result in crack propagation, steel bar corrosion, evenly durability reduction. Therefore, the reasonable assembled types (shape and assembly position) was developed and characterized, which could not only enable an appropriate inelastic deformation capacity, but also avoid cracks appearing. Frequently used connection type of precast concrete element including grouted sleeve connection (Belleri and Riva 2012, Popa *et al*. 2015), bolted connection (Kremmyda *et al*. 2014), prestressed tendon connection (Hawileh *et al*. 2010, Kim *et al*. 2010), compressed sleeve connection (Zhang *et al*. 2016) and lap connection were applied in practical projects. In particular, precast structures were connected with grouted sleeve connection guaranteed the steel continuity following the cast-in-place concrete monolithic concept.

Many references exist dealing specifically with the characterization of precast concrete column-to- foundation connections (Belleri and Riva 2012, Kim 2000, Riva 2006). The prevailing column-to-foundation jointing system consists of outcrop bars extend from the foundation and introduced into grouted sleeve in the precast column. Results from these studies, as long as they are well designed and constructed for seismic resistance, connection will exhibit strength, stiffness and ductility comparable with (and, in some case, even superior than) monolithic cast-in-place connection. However, the failure mode of the both types are significantly different and precast column-to-foundation was more susceptible to shear damage resulting

*Corresponding author, Professor
E-mail: duxiuli@bjut.edu.cn
[a]Ph.D.
E-mail: liuhongtao@bjut.edu.cn

http://www.techno-press.com/journals/easandsubpage=7
ISSN: 2092-7614 (Print), 2092-7622 (Online)

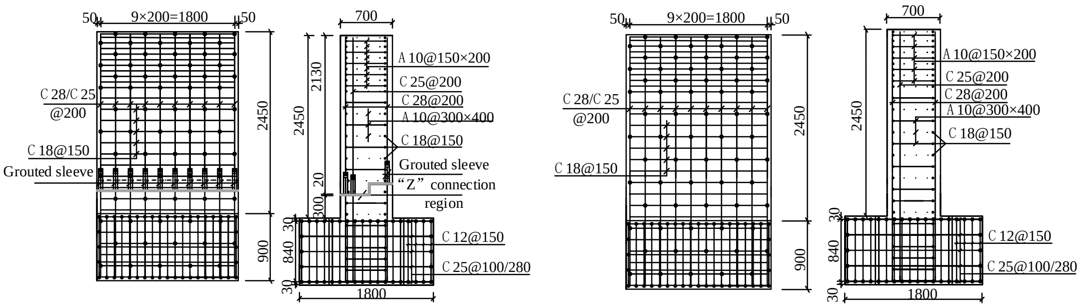

(a) Specimen PWJ (b) Specimen CWJ

Fig. 1 Dimensions and reinforcement of details of specimens (Unit:mm)

Table 1 Geometric details of the prefabricated parts

Specimens	Prefabricated parts	B×L /mm²	H/mm	Longitudinal reinforcement			Transverse reinforcement/mm		Connection type	Axial compression ratio
				Diameter/mm	Ratio/%	Spacing/mm	Diameter	Spacing		
PWJ	Sidewall	700 ×1900	2450	25/28	1.29	200	18 10	150 300×400 (150×200)	grouted sleeve	0.15
	Foundation	1800 ×1900	900	25	—	100/280	12	100		
CWJ	—	700 ×1900	2450	28/25	1.29	200	18 10	150 300×400 (150×200)	—	0.15
	—	1800 ×1900	900	25	—	100/280	12	100		

from the uncoordinated stiffness distribution. Specimens connecting with grouted corrugated steel sleeves were tested by Popa *et al*. (2015) under reversed cyclic loading protocol and the experimental results showed that the specimens had hysteresis characteristic like those expected for monolithic column under the different axial compression ratio. Similarly, tests of shear wall-to-foundation connections incorporating grouted splices subjected to reversed cyclic showed that precast shear wall joint is capable of matching overall performance of the cast-in-place connection (Soudki *et al*. 1995a, Soudki *et al*. 1995b). From the above studied, the connection seam incorporating grouted sleeve was flay type, namely, the grouted sleeve is in the same height section of precast specimen. Little effort has been sought towards different assembled sharp of precast unit. However, the connection of underground structures need complex contact surface to satisfy sufficient shear strength.

Besides that, the assembly position for precast unit was of crucial importance for the connecting performance in the case of seismic loading. Ameli *et al.* (2014) carried out an experimental study of precast column-to-foundation subjected to cyclic quasi-static loading aimed at investigating the effect of the splice sleeve location in the overall response of the test specimens. Haber *et al* (2014) taken the location of grouted sleeve within the plastic hinge zone as a test variable and results shown that the plastic hinge mechanism could be significantly affected by the grouted sleeve.

As mentioned previously, the main objectives of this study are, on one hand to discuss the distinctions of cyclic behavior with the cast-in-place sidewall joint according to the experiments, and on the other hand to study effect of joint shape and position on joint deformation performance and crack width. A full-scale precast sidewall joint incorporating grouted splice with assembled "*Z*" shape was designed and constructed, and another full-scale monolithic cast-in-place concrete specimen with identical details served as a control. Base on the experimental results, a series of numerical analysis were performed to investigate the effects of assembled location and shape. Despite the available studies for precast connection with grouted splices and even the design guidelines of precast connection for ground structures has been existed, regular practical implementation of precast structure continues to be slow. In particular, the studies for the different location and shape of assembled seam were still scarce. These results might provide valuable guidance for the constructions of underground structures with precast elements.

2. Test program

2.1 Specimen and design parameter

The research team tested a group of two specimens designated as specimens PWJ and CWJ, respectively. Specimens PWJ represented the joint with assembled monolithic subway station, and specimens CWJ represented the joint with cast-in-place subway station. The specimens were taken from connection position between sidewall and bottom slab of the station where the bending moment value is the largest and the compression ratio of specimen was 0.15 according to force state of overall station. To better

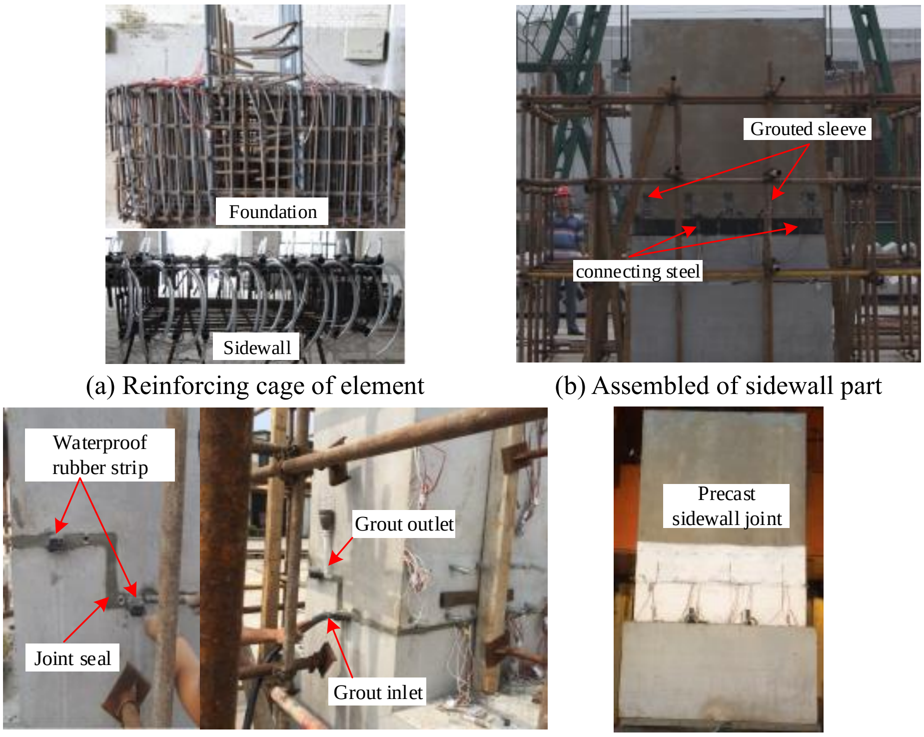

(a) Reinforcing cage of element (b) Assembled of sidewall part

(c) Grouted material (d) PWJ specimen

Fig. 2 Manufacturing operation of PWJ

Table 2 Mechanical properties of reinforcement bar obtained from material testing

Grade of steel	Diameter /mm	Yield strength /MPa	Ultimate /MPa	Yield strain/$\mu\varepsilon$	Elasticity modules/GPa
	25	454	617	2163	209
HRB400	28	420	594	2003	210
	18	436	564	2096	208
HRB335	12	475	523	1902	198
HPB300	10	307	346	1624	189

represent the behaviour of the real structure, the size of the specimens were designed as large as possible to make full use of the loading capacity of the testing equipment. Two specimens were designed with the same dimensional size (1900 mm×700 mm×2450 mm) and reinforcement details, but the structural form which mainly demonstrate the connection pattern of steel and concrete were different obviously. The steels of specimen PWJ are connected with grouted sleeve that protrude into mortar grouted coupling sleeves and the concrete connection region adopts “*Z*” type connection which could ensure the shear strength of sidewall joints. Fig. 1 and Table 1 showed the geometry, dimensions and reinforcement details of each specimens. It is noteworthy that the ribbed steel bar of grade HRB400 was used as the longitudinal reinforcing steels which included two kinds of diameter of rebar and was divided into three rows.

2.2 Material specifications

Material properties of the concrete and steel units used in the specimens were evaluated through tests of material

Table 3 Mechanical properties of cementitious grout for splices

Grand	Compression strength (average test results)/MPa			
	1d	3d	7d	28d
CGMJM-VI	41.2	68.5	88.4	100.1
CGMJM-VIII	52.5	79.6	96	118.3

samples. In the case of concrete, tests were conducted on standard cubes (150 mm×150 mm×150 mm). The average compressive strength of concrete f_{cu} was determined to be 48.0MPa. For steel, coupons were prepared and tested according to the Chinese national standard GB/T228.1-2010. The mechanical properties of steel of all specimens at the time of testing is presented in Table 2. The cementitious grout of CGMJM-VI and CGMJM-VIII were used to connect sleeve splice with bars diameter of 25 mm and 28 mm, respectively. The characteristic properties of the cementitous grout with standard cubes of 40 mm×40 mm×160 mm following the Chinese code were experimentally measured and summarized in Table 3.

2.3 Manufacturing operation of specimen

The specimen of PWJ are made up of precast foundation and sidewall uints. The fabrication process is as follows: (1) the grouted sleeve and discontinuous reinforcing bars were connected using a thread on one end, then the reinforcement cage of foundation part and sidewall part were manufactured and poured into concrete, as shown in Fig. 2(a); (2) After the foundation is set up, then waterproof rubber strip was installed at splicing joint, and the precast sidewall is assembled (the reinforcement bar of foundation

Fig. 3 Manufacturing operation of CWJ

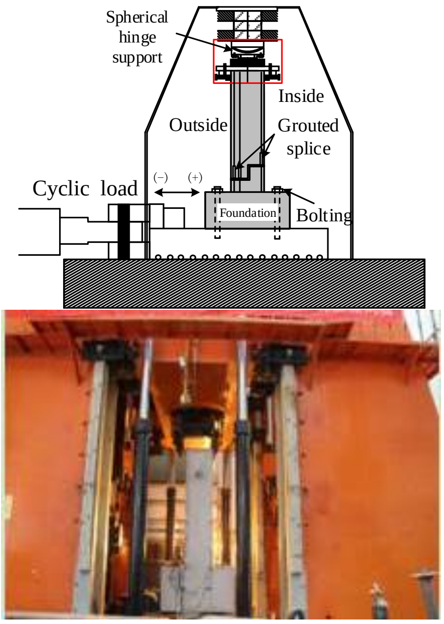

Fig. 4 Test setup

inserted into grouted sleeve of precast sidewall), as shown in Fig. 2(b); (3) Finally, grouted material were protruded into the grouted sleeve and assembled seam by means of reserved grouted hole, as shown in Fig. 2(c). The manufacturing process of CWJ was relatively simple. The reinforcement cage of foundation and sidewall was a whole and poured into concrete integrally, as shown in Fig. 3.

2.4 Test setup, instrumentation and loading sequence

The specimens were tested under horizontal reversed cyclic loading, applied in quasi-static conditions using the 40,000 kN capacity multifunctional electrohydraulic servo loading test system at the Key Laboratory of Urban Security and Disaster Engineering of Ministry of Education at Beijing University of Technology. The loading apparatuses are shown in Fig. 4. The top end of specimen was spherical hinge support. Loads applied at the bottom end of the sidewall was measured with a load cell attached in series with an actuator that applied reversed cyclic lateral load. When the outer side of the cross-section of specimen was pulled, the load was negative (-). Conversely, the load was positive (+).

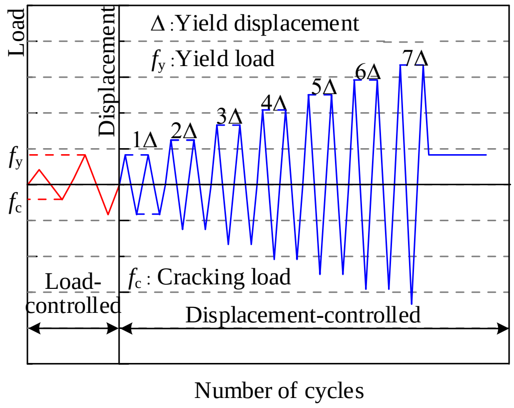

Fig. 5 Low-reversed cyclic loading law

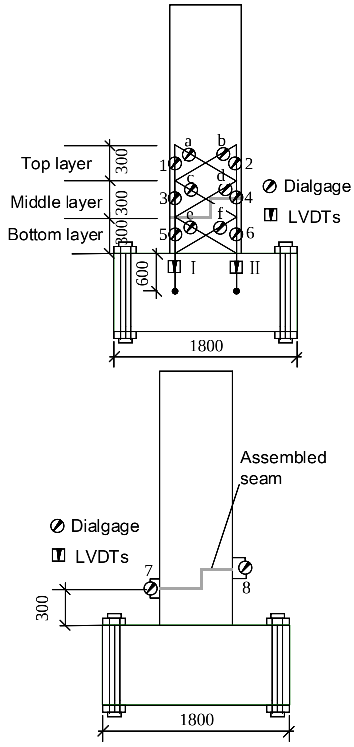

Fig. 6 Installation position of instrumentation

The axial load was applied to the sidewall through an actuator at the sidewall top, which was maintained constant during the test. The cyclic loading applied at the bottom ends of specimen was generally load-controlled at first and displacement-controlled subsequently with the increasing of yield displacement. The load-controlled loading was applied in the two cycles, and the first cycle was to get cracking load (f_c), and the second cycle was to get yielding load (f_y) and displacement (Δ) of specimen. Each load step of the displacement-controlled loading scheme consisted of two load cycles which has the same peak deformation amplitude. The specimen failure mode was identified from the loading dropped to 85% of carrying capacity. The loading history of specimen was shown in Fig. 5.

2.5 Test content and instrumentation distribution

The response quantities of interest included the shearing

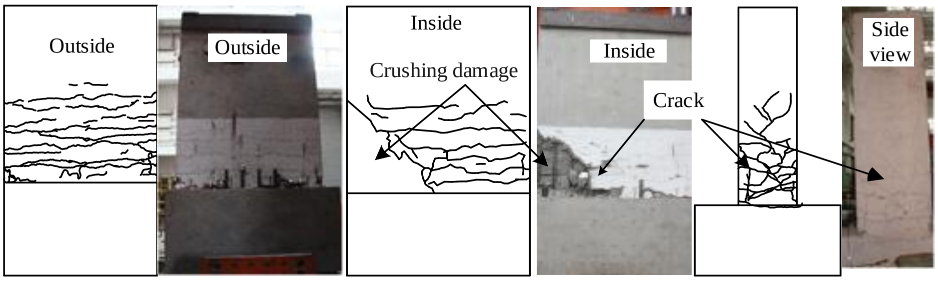

Fig. 7 Failure pattern and cracks of cast-in-suit concrete specimen (CWJ)

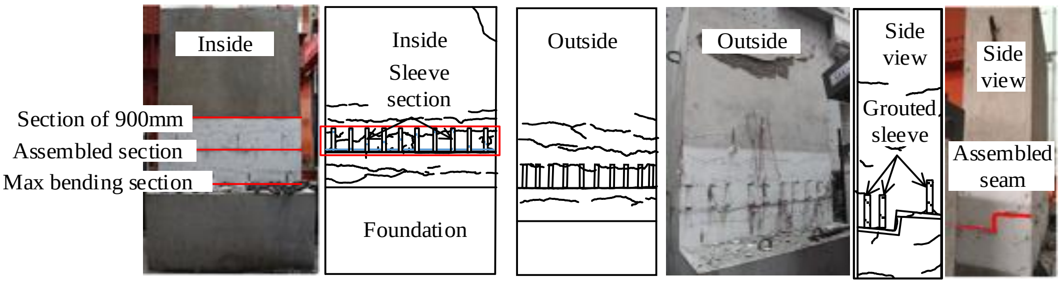

Fig. 8 Failure pattern and cracks of precast concrete specimen (PWJ)

deformation, bending deformation, slipping deformation and cracking width. Fig. 6 illustrates distribution of the dial indicators. Twelve dial indicators were stalled in the bottom of sidewall to measure the shearing and bending deformations of plastic hinge zone and two Linear Variable Displacement Transducers (LVDTs) were used to measure the slipping deformation. Two dial indicators were installed in the assembled seam of the both sides of the test specimen to measure the cracking width.

3. Experimental results and discussion

3.1 Failure patterns of specimens CWJ and PWJ

The development of crack or the crack distribution within the specimen CWJ under cyclic loading can be observed from Fig. 7. The failure status of specimen was of typical bending damage. The uniform and dense cracks were mainly distributed at plastic hinges zone. The distribution of cracks on both sides of the station was different because of the reinforcement bars were not equally distributed (single row of bars inside the station and double row of bar outside of station), as shown in Fig. 1.

From specimen of CMJ, a flexural crack first developed form the bottom surface near the foundation, which could defined as the cracking state and the load were 465.9 kN(-) and 260.1 kN(+), respectively. When the applied loading approached the yielding load (1046 kN(-) and 771 kN(+)), the width and number of cracks increased drastically, and the cracks were found within the range of 800mm at the bottom of the foundation. As the loading continued, five transverse transfixed main cracks generated and the crack at the bottom and top of specimen developed horizontally and obliquely downward, respectively. The severely damaged region was at the bottom of the specimen. According to the final failure mode of the specimen, piece of concrete fall off due to concrete crush and the reinforcement bars can be clearly seen.

The failure of the specimen PWJ envolved in a similar way, which consisted of elastic stage, cracking stage, yield stage and failure stage. It is worth noting that cracking pattern has many differences with specimen CWJ. As shown in Fig. 8, three main cracks concentrated at region of stiffness abrupt change and section of 700 and 900 mm from assembled seam. The grouted sleeve could enhance the section stiffness and the assembled seam could weaken the section stiffness, which could result in the uneven stiffness distribution. From the Fig. 8, one can see that the vertical cracks were found at the position of grouted sleeve region. The main reason of the above observations is that the bond-slip strength between the grouting sleeve and the surrounding concrete is weak, which leads to their uncoordinated deformation.

3.2 Hysteretic loading-displacement relationship

The hysteretic curves of force-displacement of sidewall-end provide important information for evaluation of seismic behavior, as shown in Fig. 9. One can see that the bearing capacity was 1200 kN (1164.7 kN) in the negative direction because of the outer side of cross-section with double bar was pulled, and lower load was observed in positive direction. The skeleton curves obtained from peak points of each cycles of hysteretic curve could reflect the yield stage, peak point and failure stage etc. It can be found that an initial response for specimens CWJ and PWJ can be considered to be linear. The specimens enters the yield state, and the loading and unloading stiffness reduced significantly with increasing deformation of sidewall-end. When the carrying capacity exceeds the peak load and before the 85% of the peak load, the second cycle loading stiffness was significantly lower than that of the first loading stiffness for the same load step.

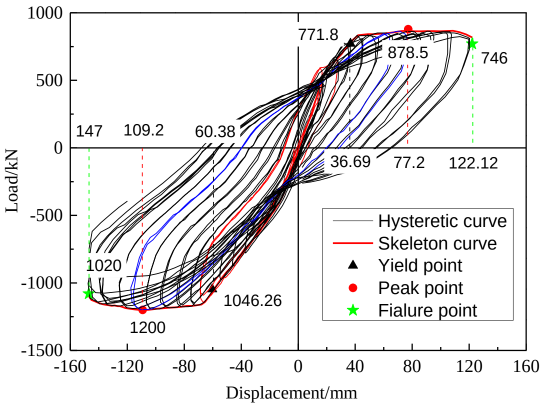

(a) Specimen CWJ

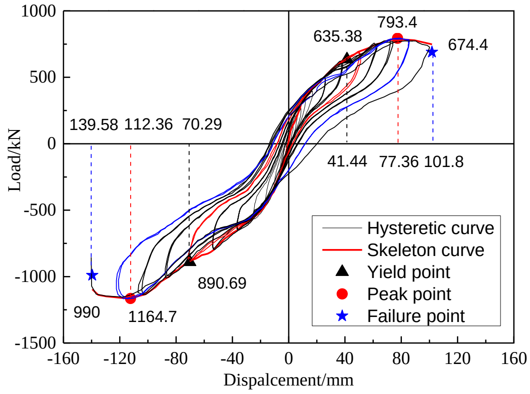

(b) Specimen PWJ

Fig. 9 Load-deformation curve of specimens

As illustrated in Figs. 9(a)-(b), the pinching behavior of specimen CWJ was more obvious than that of specimen PWJ. The bond-slip interaction of steel rebar and surrounding concrete should be the main reason for the pinching effect of hysteretic curves, and it is worth mentioning that the cracks distribution (as shown in Figa. 7 and 8)were of crucial effect for the response curves of load-deformation in the case of cyclic loading. The deformability and carrying capacity of specimen CWJ was capable of matching that of specimen of specimen PWJ, but the area of hysteretic loop of specimen CWJ was larger than that of specimen PWJ, which can be considered roughly the hysteretic energy dissipated by the precast sidewall connections was reduced. The residual deformation of specimen PWJ is significantly lower than that of specimen CWJ.

3.3 Shear displacement and bending displacement

It is well known that the bending, shearing and slipping deformation will be produced in the bottom of sidewall subjected to the low cyclic loading. The seismic energy was be absorpted and dissipated according to the bending deformation, but the shearing and slipping deformation could narrow hysteresis loop and reduce energy consumption. Therefore, reducing the shearing deformation and slipping deformation as soon as possible plays the important role in improving the seismic capacity of specimens. The shearing deformation diagram was plotted

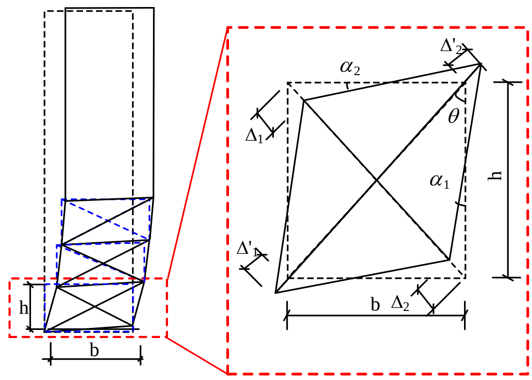

Fig. 10 Shear deformation diagram

in Fig. 10 and the theoretical shear deformation can be calculated by Eqs. (1)-(3).

$$\sin\theta = \frac{b}{\sqrt{h^2+b^2}}, \quad \cos\theta = \frac{h}{\sqrt{h^2+b^2}} \tag{1}$$

$$\alpha_1 = \frac{\sin\theta}{h}\cdot\frac{|\Delta_1+\Delta_2|+|\Delta'_1+\Delta'_2|}{2},$$
$$\alpha_2 = \frac{\cos\theta}{b}\cdot\frac{|\Delta_1+\Delta_2|+|\Delta'_1+\Delta'_2|}{2} \tag{2}$$

$$\gamma = \alpha_1+\alpha_2 = \frac{\sqrt{h^2+b^2}}{hb}\cdot\frac{|\Delta_1+\Delta_2|+|\Delta'_1+\Delta'_2|}{2} \tag{3}$$

In which, Δ_1, Δ_2, Δ'_1, Δ'_2 were the diagonal deformation of bottom layer plastic zone according to dial indicator *e* and *f*, respectively, and the dial indicator *a*, *b* and *c*, *d* could get the diagonal deformation of each layer; *h*, *b* were the section height and width of each layer, respectively.

3.3.1 Shearing deformation

The shear angle versus deformation relationship can be described as presented in Fig. 11. The horizontal axis represents the loading displacement of the sidewall-end, and the vertical axis represents the shear angle of each layer of the plastic hinge zone at the bottom of the sidewall, which could be calculated by Eqs. (1)-(3). In general, the shear angle of each layer increases with increasing displacement of the sidewall-end, but there exits obvious differences between the shearing deformation of specimens CWJ and PWJ, which mainly reflected in the following three aspects. (1) From Fig. 11(a), one can see that the increase of shear angle is not obvious when the deformation of sidewall-end is less than 50 mm which can be considered roughly as the yield point, and the shear angle increase obviously after yield point. However, for specimen PWJ, the shear angle increases monotonously with respective to the applied load of sidewall-end, as shown in Fig. 11(b). (2) The shearing deformation of specimen PWJ is significantly smaller than that of specimen CWJ because of the failure modes of specimens were different obviously. (3) The shearing deformation at the bottom layer of specimen CWJ is the largest and gradually reduced along the height of specimen; but the shearing deformation of the middle layer of the specimen PWJ is the largest, which is mainly related to the assembled seam.

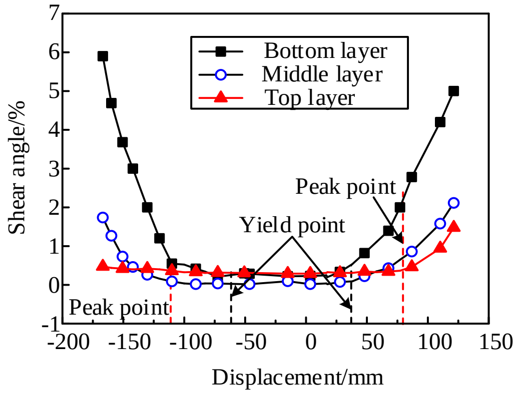

(a) Specimen CWJ

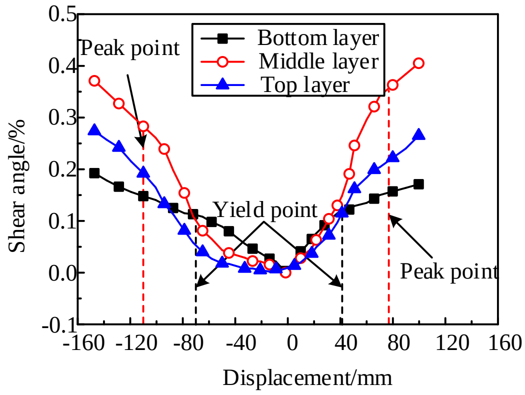

(b) Specimen PMJ

Fig. 11 Shear angle-deformation curves

3.3.2 Bending deformation

Bending deformation is an important way to increase the ductility of components. The bending angle φ could be calculated by Eq.(4), and δ_1, δ'_1 were the each layer vertical deformation of both sides of the specimen, which could be measured by dial indicator 5 and 6, as shown in Fig. 6. The bending angle of different layer of specimens CWJ and PWJ were compared in Fig. 12.

$$\varphi = \frac{\delta_1 - \delta'_1}{b} \tag{4}$$

The specimen CWJ is capable of sustaining at least 50 mm deformation without a significant increase in bending angle. For the specimen PWJ, the bending angle increases monotonously with respective to the applied load of sidewall-end, and the platform stage performance is not obvious, as shown in Fig. 12(b). The most obvious differences were mainly reflected in the following two aspects. (1) The bending angles at different positions (bottom layer, middle layer and top layer) were different, and the overall deformation of specimen CWJ is significantly larger than that of specimen PWJ. (2) The bending angle of specimens at the same positions is different because of the different assembled forms and configurations. For the specimen of CWJ, the bending angle of bottom layer is the largest and the bending angle shown a downward trend from bottom layer to top layer, which illustrated the proportion of bending deformation is very large in the bottom layer. However, the middle layer bending angle of specimen PWJ is the largest. The essential cause is uncoordinated stiffness distribution.

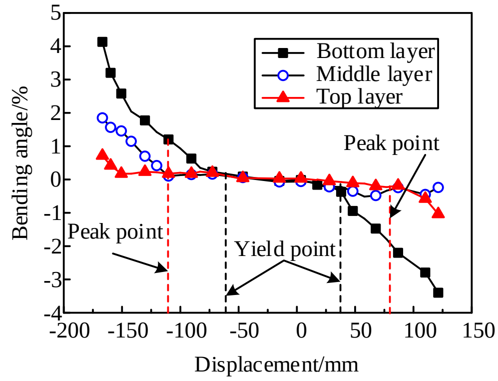

(a) Specimen CWJ

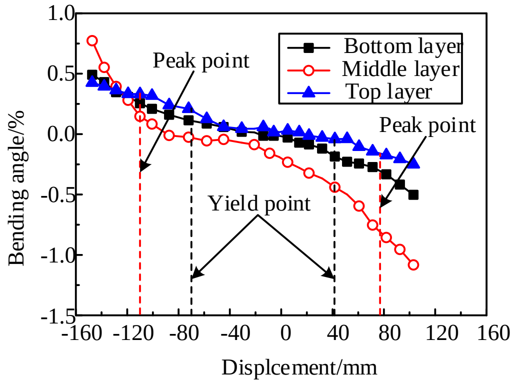

(b) Specimen PMJ

Fig. 12 Bending angle–deformation curves

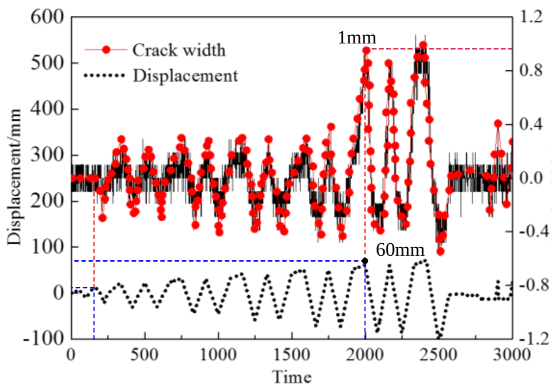

Fig. 13 Cracking width process

3.4 Crack width of assembled seam

Cracks can deteriorate mechanical properties and destabilize a concrete structure, regardless of size or type. For underground concrete structures, the presence of water could corrode steel bar and influence usage function and durability of structure. The assembled seam is probably inevitable for the precast concrete structures, which is the weakest part of the tension. So the cracking width of assembled seam (see Fig. 6) under reversed cyclic loading was measured. According to Fig. 13, the cracking do not appear at the assembled seam location in the elastic phase

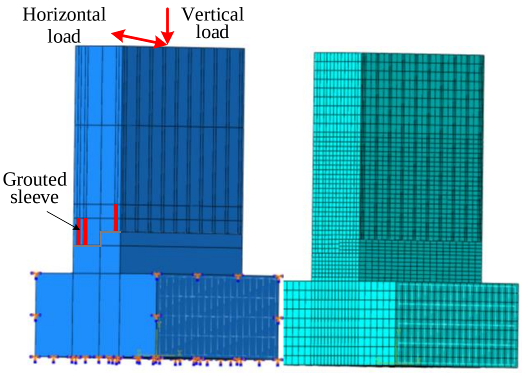

Fig. 14 Boundary conditions and FEM model of specimens

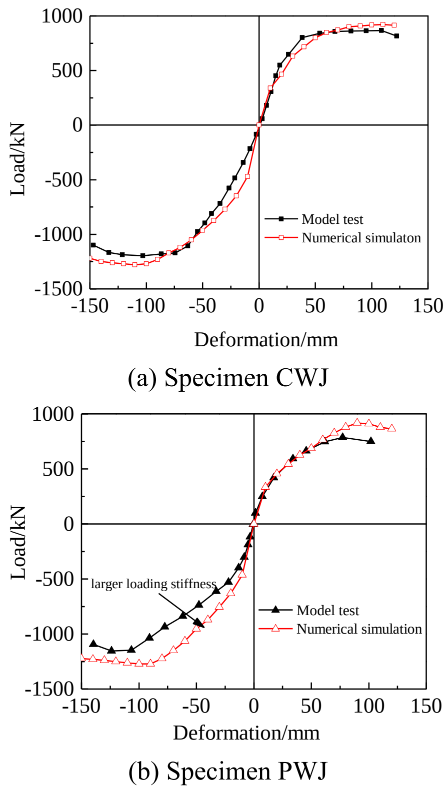

Fig. 15 Comparison of skeleton curve

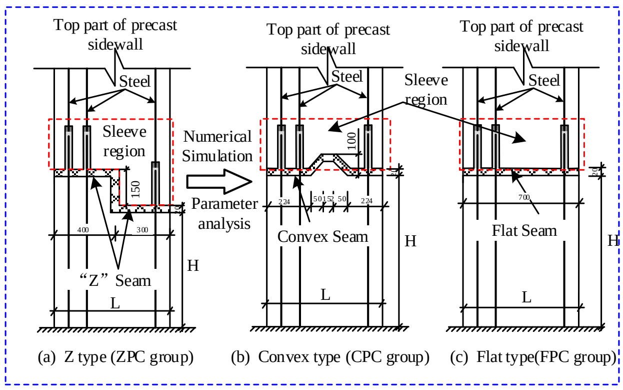

Fig. 16 Parameter analysis model and seam construction

and the cracking rapidly expensed when the deformation of sidewall-end was 60mm. the maximum cracking width of assembled seam was about 1mm,which was not allowed for the underground structure (Pantelides *et al*. 2003).

4. Model calibration for sidewall joint

Accurate and efficient nonlinear element model and associated material model are critical issue to be considered in simulating connection performance. This quasi-static experiment is also capable of efficiently and reliably presenting the key seismic characteristics of specimen CWJ and PWJ, thereby laying a foundation for the further comparison of different design schemes using finite elements method adopted by ABAQUS. In order to accurately simulate the forcing characteristics for the grouted sleeve and assembled seam region, the concrete and steel bar were modelled with standard solid continuum elements with reduced integration and truss element, respectively. The plastic damage modelling concrete and ideal plastic modelling steel are utilized to capture the mechanical properties of sidewall joint, but do not consider the bond-slip interaction of steel rebar and surrounding concrete. Three-dimensional numerical models with the same dimensions and "*Z*" connection type as the experimental models was established as shown in Fig. 14.

The foundation was fixed and the vertical and horizontal monotonous loading was applied on the top of sidewall. From the numerical analysis model, the skeleton curve of specimen was presented to compare carrying capacity and deformability. In order to improve the computational efficiency, the grouted sleeve and cementitious grout were simplified to the ideal elastic-plastic material according to the uniaxial tensile test (Liu *et al*. 2018). The interaction properties were of crucial importance for the efficiency of the model especially in the case of cyclic loading, so the cohesive elements were utilized to express the mechanical properties of the contact surface.

The comparison between the experimental data and the simulation results were compared in Fig. 15. One can see that global behavior of specimen could be simulated to correlate with the experimental observations. However, the carrying capacity of simulation was about 10% more than test value because of the cumulative damage of cycling load was ignored. For the specimen PWJ, the loading stiffness of numerical simulation was larger than that of model test in the last loading stage.

5. Heights and shapes of assembled seam study

The heights and shapes of assembled seam were of crucial importance for the mechanical properties and construction convenience of precast assembled structures. The height ratio was defined as $\delta=H/L$. Herein, H means the distance from assembled seam to foundation, and L means width of section. Seven sets of height ratio (0, 0.14, 0.28, 0.43, 0.57, 0.86 and 1.14) and three variably-shape (Flat type, *Z* type and convex type) were considered, as shown in Fig. 16. The carrying capacity, deformability and width crack were presented in Section 5.1 and Section 5.2. In

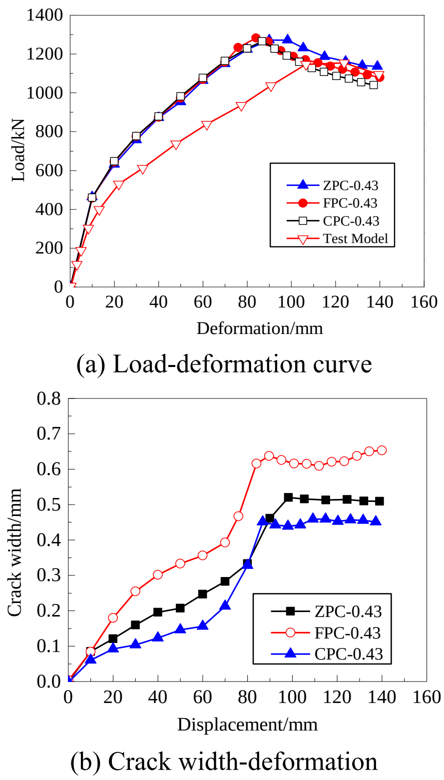

(a) Load-deformation curve

(b) Crack width-deformation

Fig. 17 Effect analysis of assembled seam shape

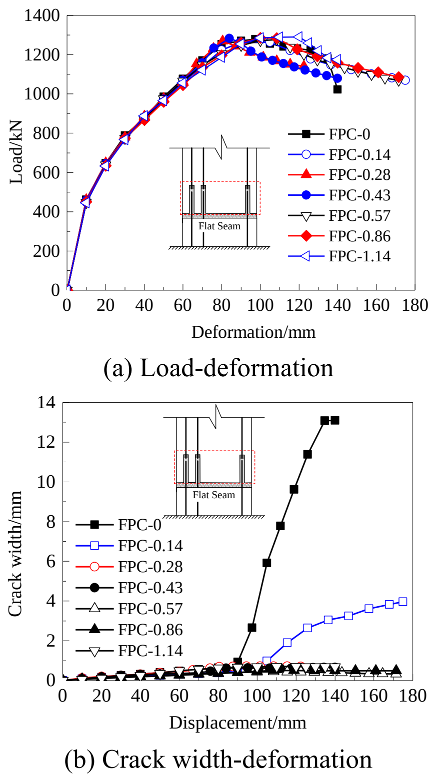

(a) Load-deformation

(b) Crack width-deformation

Fig. 18 Effect analysis of FPC group

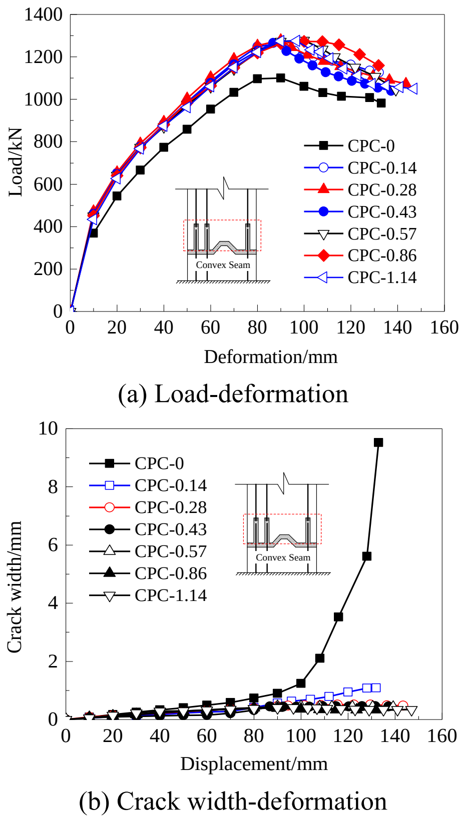

(a) Load-deformation

(b) Crack width-deformation

Fig. 19 Effect analysis of CPC group

addition, the name of three groups of specimen was dented as FPC-xx, ZPC-xx and CPC-xx. Namely, the FPC, ZPC and CPC represent the specimen with different connection of flat type, *Z* type and convex type, respectively. The xx were the height ratio.

5.1 Effect of assembled seam shape

Take one of height ratio 0.43 as an example, the carrying capacity, deformation and crack width of different assemble seam shape were depicted in Fig. 17.

The Fig. 17(a) illustrates the relationships between load and deformation of sidewall-end from monotonous loading to compare the differences of carrying and deformation capacity. One can note that the load-deformation curve evolves similarly for the all specimens. That is to say, the carrying capacity increases first and then decreases with increasing of deformation sidewall-end. Nevertheless, one can see that the computational initial stiffness was obviously larger than that of test model. Additionally, the main influence of different assembled seam shape on the seismic performance concentrated mainly in the later loading stage.

The crack width of assembled seam versus deformation of sidewall-end relationship can be described as presented in Fig. 17(b). It can be noted that the crack width for the all specimens have an increasing trend with deformation increasing before peak load, after the crack width basically remain the same. While the maximum and minimum crack width were found in the specimen connected by flat type and convex type, respectively. Compared to the crack width of test model, the computational crack width is about 45% than that of test model because of the bond-slip interaction of steel rebar and surrounding concrete near the assembled seam was not considered.

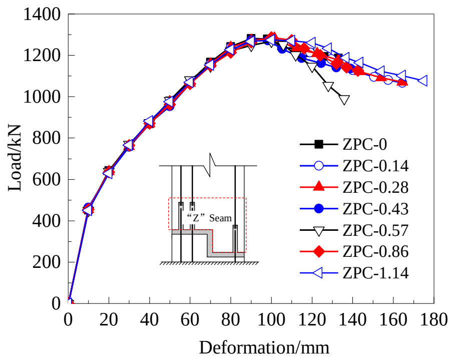

(a) Load-deformation

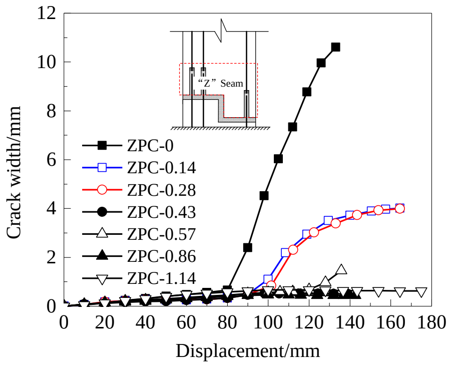

(b) Crack width-deformation

Fig. 20 Effect analysis of ZPC group

5.2 Effect of assembled seam height

An important subject in considering the location of grouted splices is then relationship with respect to the deformation mechanism and carrying capacity expected for the study. Fig. 18 illustrates the relationships carrying capacity or crack width and the deformation for specimens connected with flat type.

Fig. 18(a) shows that the influence of location of splices on carrying capacity is not obvious and the significant distinction of strength degradation was observed after the peak load. From the Fig. 18(b) one can see that the crack width of precast member connecting location reduces with increasing height of assembled seam for the flat type. The crack width was about 13 mm when the height ratio was 0 and the crack width tends to be consistent (less than 1 mm) when the height ratio was greater than 0.28.

For specimens connected with convex type, as shown in Fig. 19, the carrying capacity of CPC-0 was up to 15% lower than that of others, and the crack width was 9 mm, which was largest in the specimens connected with convex type. When the height ratio was greater than 0.28, the crack width was less than 1 mm. Additionally, the specimen of *Z* type adopted in the experimental study, which was easy to be installed in actual practice, demonstrated structural behavior similar to those of convex type and flat type. The crack width of the simulation results were consistent with the test results that both of the crack width in specimen ZPC-0.43 was lower than 1mm. It is worth mentioning that the crack width of specimen ZPC-0.28 was obviously larger than that of the others connected with convex and flat type, as shown in Fig. 20.

This definitely indicates that the location of splices has no obvious influence on the carrying capacity and deformation capacity of the precast specimen. However, the location of assembled seam were of crucial importance for crack width especially in the case of underground structures. As a result, the location of splices should be avoided at the bottom of the precast members and the height of splices from top of footing should be 0.5 times the width of the section.

6. Conclusions

This paper present the experimental investigation on the seismic behavior of precast sidewall joints, failing in bending mode under low-reversed cyclic loading. The cast-in-place sidewall joint and precast joint were evaluated and compared in term of failure pattern, loading carrying capacity, deformation performance and crack width. The assembled seam height and shape for the precast sidewall joints were explored and discussed. Based on the experimental studies and numerical parameter analysis, the following conclusion can be draw:

- The precast sidewall with capable of sufficient strength and deformation capacity demonstrated structural behavior similar to those of cast-in-place sidewall joints, but the crack distribution were different obviously. Compared to failure mode of precast sidewall joint, the failure crack of precast sidewall joints always concentrated in stiffness abrupt region.
- The bending deformation and shearing deformation in the plastic hinge zone have significantly different trends. The assembled seam of precast sidewall joints and the bottom of the plastic zone were changed obviously, respectively.
- The crack width of assembled seam for the precast sidewall joints were about 1mm, which is unfavorable for normal use of underground structures. In extremis, the steel will be rusted, which result in connection failure of precast member.
- The shape of assembled seam has significant influence for the crack width and carrying capacity in the post-critical stage. The crack width of assembled seam with flat type was most unfavorable. The connection with convex type were usually recommended for the precast sidewall joint.
- With the increase of assembled seam height, the crack width of assembled seam was reduced. When the assembled seam was placed in bottom of precast sidewall unit, the crack width is the most unfavorable. So the height of the assembled seam is at least about 0.5 times the width of the section can be suggested for the design of precast underground concrete structures.

Acknowledgments

This work was supported by the National Natural Science Foundation of China (No.51421005, 51908013) and the National Key Basic Research and Development

Program of China (No.2018YFC1504302). Their supports are gratefully acknowledged.

References

Akköse, M., Sunca, F. and Türkay, A. (2018), "Pushover analysis of prefabricated structures with various partially fixity rates", *Earthq. Struct.*, **14**(1), 21-32. https://doi.org/10.12989/eas.2018.14.1.021.

Ameli, M.J., Parks, J.E. Brown, D.N. and Pantelides, C.P. (2014), "Grouted splice sleeve connection alternatives for precast reinforced concrete bridge piers in moderate-to-high seismic regions", *NCEE 2014 - 10th U.S. National Conference on Earthquake Engineering: Frontiers of Earthquake Engineering*, Earthquake Engineering Research Institute, Anchorage.

Beilic, D., Casotto, C., Nascimbene, R., Cicola, D. and Rodrigues, D. (2017), "Seismic fragility curves of single storey RC precast structures by comparing different Italian codes", *Earthq. Struct.*, **12**(3), 359-374. https://doi.org/10.12989/eas.2017.12.3.359.

Belleri, A. and Riva, P. (2012), "Seismic performance and retrofit of precast concrete grouted sleeve connections", *PCI J.*, **57**, 97-109.

Choi, H.K., Choi, Y.C. and Choi, C.S. (2013), "Development and testing of precast concrete beam-to-column connections", *Eng. Struct.*, **56**, 1820-1835. https://doi.org/10.1016/j.engstruct.2013.07.021.

Haber, Z.B., Saiidi, M.S. and Sanders, D.H. (2014), "Seismic performance of precast columns with mechanically spliced column-footing connections", *ACI Struct. J.*, **111**(3), 639-650.

Hawileh, R.A., Rahman, A. and Tabatabai, H. (2010), "Nonlinear finite element analysis and modeling of a precast hybrid beam-column connection subjected to cyclic loads", *Appl. Math. Model.*, **34**(9), 2562-2583. https://doi.org/10.1016/j.apm.2009.11.020.

Kim, T.H., Lee, H.M. Kim, Y.J. and Shin, H.M. (2010), "Performance assessment of precast concrete segmental bridge columns with a shear resistant connecting structure", *Eng. Struct.*, **32**(5), 1292-1303. https://doi.org/10.1016/j.engstruct.2010.01.007.

Kim, Y.M. (2000), "A study of pipe splice sleeves for use in precast beam-column connections", MA. Sc. Dissertation, University of Texas, Dallas, Austin.

Kremmyda, G.D., Fahjan, Y.M. and Tsoukantas S.G. (2014), "Nonlinear FE analysis of precast RC pinned beam-to-column connections under monotonic and cyclic shear loading", *Bull. Earthq. Eng.*, **12**(4), 1615-1638. https://doi.org/10.1007/s10518-013-9560-2.

Liu, H.T., Han, Q., Bai, Y.L., Xu, C.X. and Du, X.L. (2018), "Connection performance of restrained deformed grouted sleeve splice", *Adv. Struct. Eng.*, **21**(3), 488-499. https://doi.org/10.1177/1369433217719987.

Ma, C., Lu, D.C. and Du, X.L. (2018), "Effect of buried depth on seismic response of rectangular underground structures considering the influence of ground loss", *Soil Dyn. Earthq. Eng.*, **106**, 278-297. https://doi.org/10.1016/j.soildyn.2017.12.021.

Nzabonimpa, J.D. and Hong, W. (2019), "Experimental and nonlinear numerical analysis of precast concrete column splices with high-yield metal plates", *J. Struct. Eng.*, **145**(2), 1-15. https://doi.org/10.1061/(ASCE)ST.1943-541X.0002233.

Pantelides, C.P., Reaveley, L.D. and McMullin, P.W. (2003), "Design of CFRP composite connector for precast concrete elements", *J. Reinf. Plast. Compos.*, **22**(15), 1335-1351. https://doi.org/10.1177/073168403035581.

Park, R. (1995), "A perspective on the seismic design of precast concrete structures in new zealand", *PCI J.*, **40**(3), 40-59.

Popa, V., Papurcu, A., Cotofana, D. and Pascu, R. (2015), "Experimental testing on emulative connections for precast columns using grouted corrugated steel sleeves", *Bull. Earthq. Eng.*, **13**(8), 2429-2447. https://doi.org/10.1007/s10518-014-9715-9.

Rave-Arango, J.F., Blandón, C.A., Restrepo, J.I. and Carmona, F. (2018), "Seismic performance of precast concrete column-to-column lap-splice connections", *Eng. Struct.*, **172**, 687-699. https://doi.org/10.1016/j.engstruct.2018.06.049.

Riva, P. (2006), "Seismic behaviour of precast column-to-foundation grouted sleeve connections", *International Conference on Advances in Engineering Structures, Mechanics and Construction*, Springer Netherlands, Ontario.

Soudki, K.A., Rizkalla, S.H. and Daikiw, R.W. (1995a), "Horizontal connections for precast concrete shear walls subjected to cyclic deformations part 2: prestressed connections", *PCI J.*, **40**(5), 82-96.

Soudki, K.A., Rizkalla, S.H. and LeBlanc, B. (1995b), "Horizontal connections for precast concrete shear walls subjected to cyclic deformations part 1: mild steel connections", *PCI J.*, **40**(4), 78-96.

Zhang, W.J., Guo, Y.Y. and Liu, S.W. (2016), "Experimental research on seismic behavior of precast RC columns with steel bars spliced by compressive sleeves", *Eng. Mech.*, **33**(12), 119-127.

KT